Design Proposal: Mach-Zehnder Interferometer

ARTUR SILVA[1]

[1] *PHIX B.V., Hengelosestraat 525, 7521AG. Enschede - The Netherlands*
[*] *artur.araujobg@gmail.com*

Abstract: This report details the design of a set of Mach-Zehnder interferometers (MZIs) on a silicon-on-insulator (SOI) platform. We present the theory of MZI operation, detail the waveguide and component modeling performed in Lumerical MODE and INTERCONNECT, and propose a series of design variations with different path length imbalances.

1. Introduction

Integrated silicon photonics has become a fundamental component of modern high-bandwidth optical communication systems. A notable benefit of this platform is its capacity to facilitate the fabrication of complex optical circuits on a compact chip. The Mach-Zehnder Interferometer (MZI) is among the most fundamental components in this field. It is essential for the construction of devices such as optical modulators, switches, and wavelength filters [1].

The objective of this project is to design a set of simple MZI circuits. The designs will be constrained to ensure ease of fabrication with the available E-beam lithography process. This report presents the theoretical framework, the component modeling, and the circuit design variations that will be utilized to achieve this objective.

2. Theory

An MZI operates by splitting input light into two separate paths (arms) and then recombining them, as depicted in the schematic in Fig. (1). If an optical path difference exists between the arms, the recombined light will interfere, leading to an output intensity that is highly dependent on the wavelength.

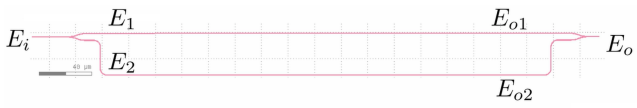

Fig. 1. Conceptual schematic of an unbalanced Mach-Zehnder Interferometer. The input field E_i is split into two arms of length L_1 and L_2 before recombining to produce the output field E_o [1].

Assuming the first Y-branch is an ideal 3-dB splitter, the input electric field, E_i, is divided equally into the upper and lower arms. As the fields propagate along their respective paths of length L_1 and L_2, they accumulate both a phase shift and attenuation. The electric fields just before the second Y-branch, E_{o1} and E_{o2}, can be described by:

$$E_{o1} = \frac{E_i}{\sqrt{2}} e^{-i\beta_1 L_1 - \frac{\alpha_1}{2} L_1} \tag{1}$$

$$E_{o2} = \frac{E_i}{\sqrt{2}} e^{-i\beta_2 L_2 - \frac{\alpha_2}{2} L_2} \tag{2}$$

where α_1 and α_2 are the attenuation coefficients for each arm. The propagation constants, β_1 and β_2, are defined as:

$$\beta_1 = \frac{2\pi n_1}{\lambda} \tag{3}$$

$$\beta_2 = \frac{2\pi n_2}{\lambda} \tag{4}$$

where n_1 and n_2 are the effective refractive indices of the respective waveguide modes. At the second Y-branch, the fields coherently combine, resulting in a total output field E_o:

$$E_o = \frac{1}{\sqrt{2}}(E_{o1} + E_{o2}) = \frac{E_i}{2}\left(e^{-i\beta_1 L_1 - \frac{\alpha_1}{2}L_1} + e^{-i\beta_2 L_2 - \frac{\alpha_2}{2}L_2}\right) \tag{5}$$

Since optical intensity is proportional to the square of the electric field magnitude ($I \propto |E|^2$), the general expression for the output intensity I_o is:

$$I_o = \frac{I_i}{4}\left|e^{-i\beta_1 L_1 - \frac{\alpha_1}{2}L_1} + e^{-i\beta_2 L_2 - \frac{\alpha_2}{2}L_2}\right|^2 \tag{6}$$

For the purpose of this design, we can simplify this general expression by assuming the waveguides are ideal and lossless, meaning $\alpha_1 = \alpha_2 = 0$. In our specific case, the waveguides in both arms are also designed to be identical, so $n_1 = n_2 = n_{\text{eff}}$ and therefore $\beta_1 = \beta_2 = \beta$. The interference is created solely by a physical path length difference, $\Delta L = L_2 - L_1$. Under these conditions, Equation 6 simplifies significantly:

$$I_o = \frac{I_i}{2}[1 + \cos(\beta \Delta L)] \tag{7}$$

This relationship can also be expressed in terms of the total phase difference between the arms, $\Delta\phi$. The normalized transfer function is then given by:

$$\frac{I_{\text{out}}}{I_{\text{in}}} = \cos^2\left(\frac{\Delta\phi}{2}\right) \tag{8}$$

where the phase difference $\Delta\phi$ is directly related to the physical path length difference ΔL by:

$$\Delta\phi = \beta \Delta L = \frac{2\pi n_{\text{eff}}}{\lambda}\Delta L \tag{9}$$

Here, n_{eff} is the effective index of the waveguide mode and λ is the vacuum wavelength. The periodic nature of this function gives rise to a transmission spectrum with distinct peaks and nulls, which is the key characteristic we will use for our analysis.

2.1. Free Spectral Range (FSR) and Group Index Extraction

The wavelength spacing between two adjacent transmission peaks is known as the **Free Spectral Range (FSR)**. It is determined by the condition that the total phase difference changes by 2π. The FSR is related to the group index (n_g) and the path length difference (ΔL) by the expression:

$$FSR = \frac{\lambda^2}{n_g \Delta L} \tag{10}$$

3. Modelling and Simulation

3.1. Waveguide Design and Modal Analysis

To ensure easy-to-fabricate designs, a standard **strip waveguide** geometry was chosen. The fabrication process defines a fixed height of **220 nm**. A width of **500 nm** was selected as it

provides strong confinement and ensures single-mode operation for the fundamental **quasi-TE polarization** in the C-band, which is the target for this design.

A simulation of this waveguide cross-section was performed to find its modal properties using a commercial solver [2].

- **Waveguide Geometry:** 500 nm (width) x 220 nm (height)
- **Polarization:** Quasi-TE
- **Simulated Mode Profile:** The fundamental TE mode is well-confined to the silicon core, which minimizes bending loss and substrate leakage, the result of the MODE simulation using Lumerical is shown in Fig. (2).

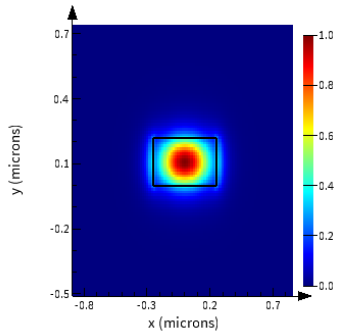

Fig. 2. Simulated E-field intensity of the fundamental TE mode, illustrating the strong optical confinement within the silicon core.

3.2. Waveguide Dispersion and Compact Model

A wavelength sweep from 1500 nm to 1600 nm was simulated to determine the chromatic dispersion of the waveguide. The resulting effective index (n_{eff}) and group index (n_g) are plotted in Fig. (3).

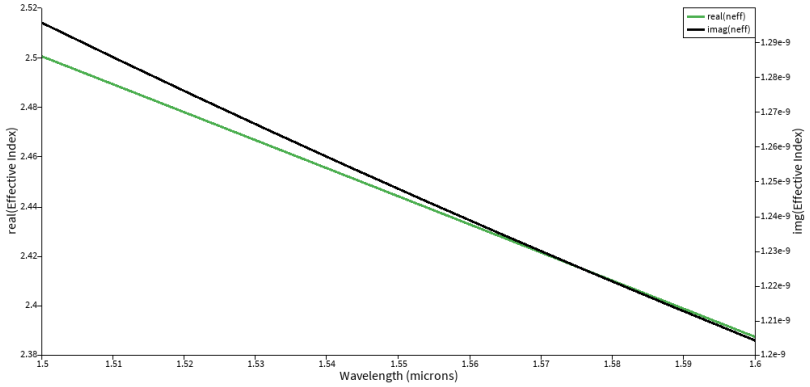

Fig. 3. Simulated effective index (real and imaginary parts) and group index versus wavelength for the fundamental TE mode.

To use these data in circuit simulations, a **compact model** considering a truncated Taylor-series (with three coefficients), the effective index can be modeled as (11).

$$n_{\text{eff}}(\lambda) = 2.4468 - 1.133(\lambda - 1.55) - 0.046(\lambda - 1.55)^2 \tag{11}$$

where λ is the wavelength in microns. Fig. (4) shows the agreement between the simulated effective index data and the Taylor-Series fit.

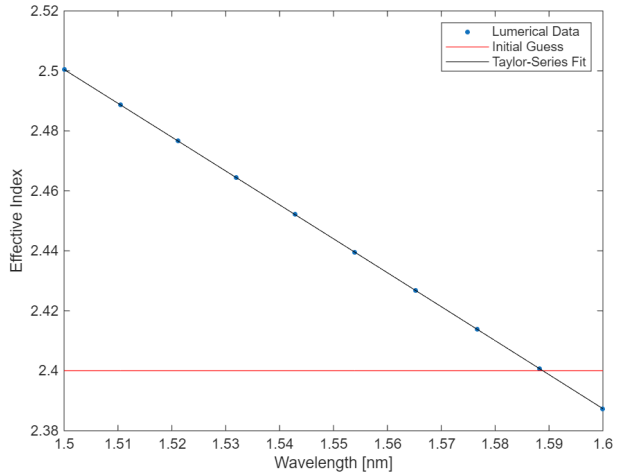

Fig. 4. Comparison of simulated effective index data points with the Taylor-Series fit.

3.3. Circuit Simulation Setup

To simulate the full circuit performance, the MZI was constructed in Lumerical INTERCONNECT, as shown in the schematic in Fig. (5). The model utilizes S-parameter data for the grating couplers and Y-branches provided by this course, combined with model simulations in the previous section.

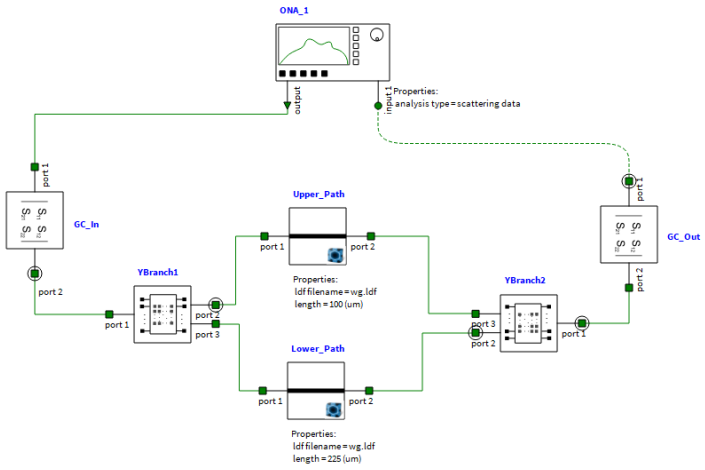

Fig. 5. Circuit schematic of the MZI in Lumerical INTERCONNECT.

The transmission spectrum for a pair of input/output grating couplers is shown in Fig. (6), indicating a peak coupling efficiency around 1550nm and a expected insertion loss of around 5dB.

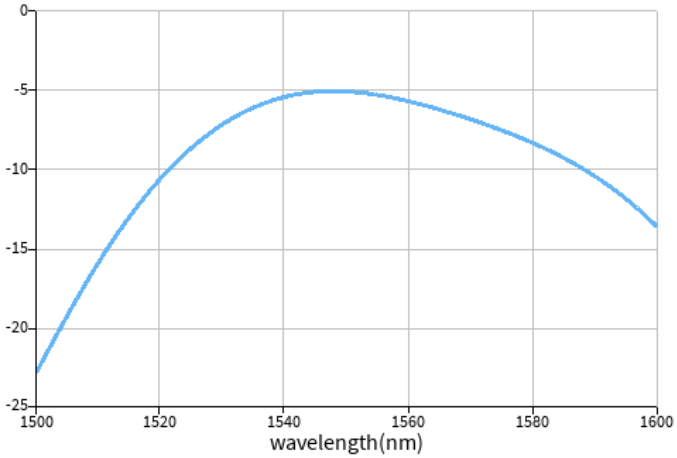

Fig. 6. Simulated transmission spectrum of an input/output grating coupler pair.

Similarly, the simulated spectrum for the Y-branch splitter in Fig. (7) shows a low, broadband insertion loss, around 3dB.

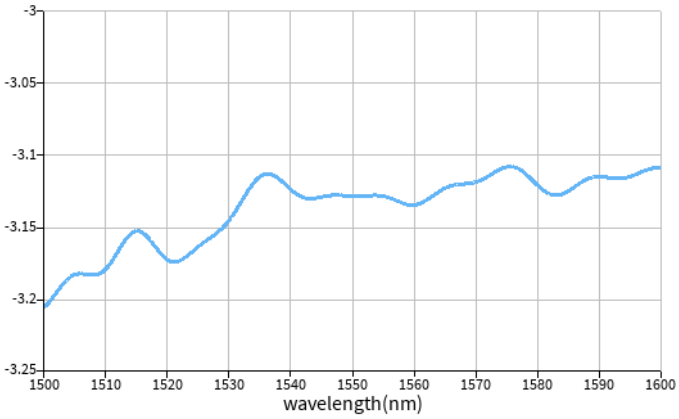

Fig. 7. Simulated transmission spectrum of a Y-branch splitter.

3.4. MZI Design Variations

To study the relationship between path difference and FSR, and to provide multiple data points for an accurate group index extraction, five MZI designs are proposed. Each design uses an identical waveguide cross-section and Y-branch splitters, with the only variation being the path length difference (ΔL).

The table below lists the design parameters and the theoretically expected FSR at a center wavelength of 1550 nm, calculated using the simulated group index value of $n_g \approx 4.197$ at that wavelength.

Table 1. MZI Design Parameters and Expected Performance

Design #	Waveguide Width	Polarization	ΔL (µm)	Expected FSR (nm)
1	500 nm	TE	25	22.89
2	500 nm	TE	50	11.45
3	500 nm	TE	75	7.63
4	500 nm	TE	100	5.72
5	500 nm	TE	125	4.58

The simulated transmission spectra for all five MZI designs are overlaid in Fig. (8), clearly showing how the Free Spectral Range (FSR) decreases as the path length difference (ΔL) increases.

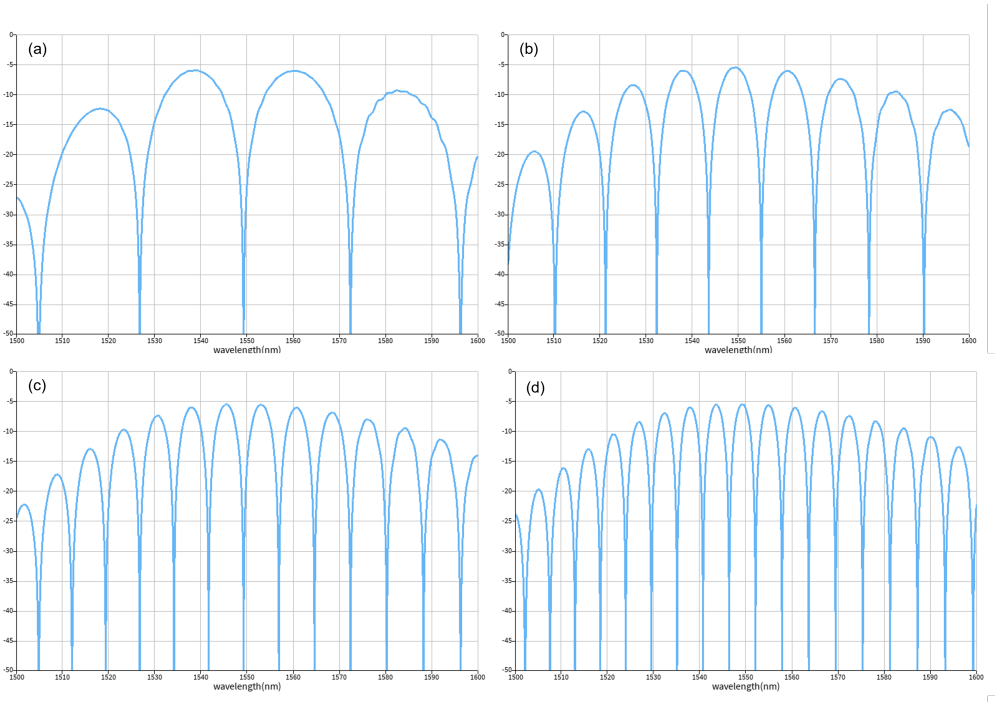

Fig. 8. Simulated transmission spectra for all MZI designs with varying ΔL. (a) $\Delta L = 25\mu m$, (b) $\Delta L = 50\mu m$, (c) $\Delta L = 75\mu m$ and (d) $\Delta L = 100\mu m$

4. Layout

The circuit designs modeled in Section 3.4 were translated into a physical layout mask using KLayout. The final mask design includes reference structures for normalization (straight waveguides with two grating couplers and two waveguides coupled to a Y-branch) and the five variations of the Mach-Zehnder Interferometer (MZI) detailed in Table 1.

To facilitate automated testing, a standard pitch of 127 μm was utilized for the input and output grating couplers, ensuring compatibility with standard fiber arrays. The grating couplers were

oriented for TE polarization. To minimize bend losses while maintaining a compact footprint, a bend radius of 5 μm was chosen for all waveguide bends. This radius is sufficient for the high-confinement strip waveguides (500 nm $\times$ 220 nm) used in this design.

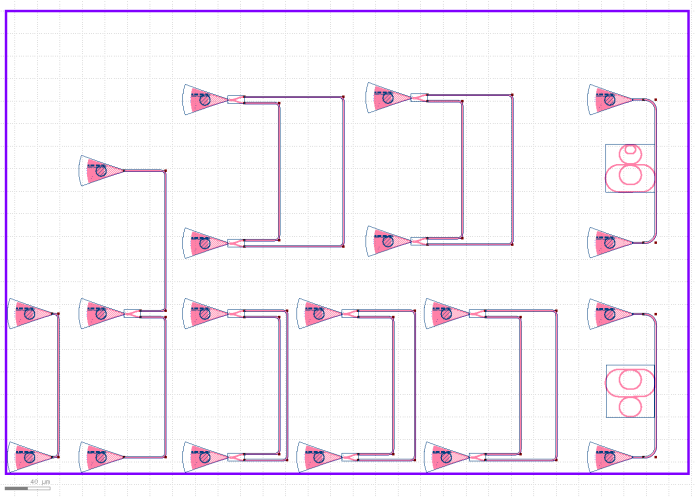

Fig. 9. Final mask layout designed in KLayout. The design includes five MZI variations and reference structures for calibration.

The final layout consists of:

- **Reference Structures:** Straight waveguides used for baseline correction and insertion loss estimation.
- **MZI Array:** Five MZI devices with path length differences (ΔL) of 25, 50, 75, 100, and 125 µm.

5. Fabrication

The photonic devices were fabricated using the NanoSOI MPW fabrication process by Applied Nanotools Inc. (Edmonton, Canada) which is based on direct-write 100 keV electron beam lithography technology. Silicon-on-insulator wafers of 200 mm diameter, 220 nm device thickness and 2 µm buffer oxide thickness are used as the base material for the fabrication. The wafer was pre-diced into square substrates with dimensions of 25x25 mm, and lines were scribed into the substrate backsides to facilitate easy separation into smaller chips once fabrication was complete.

After an initial wafer clean using piranha solution (3:1 H_2SO_4:H_2O_2) for 15 minutes and water/IPA rinse, hydrogen silsesquioxane (HSQ) resist was spin-coated onto the substrate and heated to evaporate the solvent. The photonic devices were patterned using a JEOL JBX-8100FS electron beam instrument at The University of British Columbia. The exposure dosage of the design was corrected for proximity effects that result from the backscatter of electrons from exposure of nearby features. Shape writing order was optimized for efficient patterning and minimal beam drift.

After the e-beam exposure and subsequent development with a tetramethylammonium sulfate (TMAH) solution, the devices were inspected optically for residues and/or defects. The chips were then mounted on a 4" handle wafer and underwent an anisotropic ICP-RIE etch process using chlorine after qualification of the etch rate. The resist was removed from the surface of the devices using a 10:1 buffer oxide wet etch, and the devices were inspected using a scanning electron microscope (SEM) to verify patterning and etch quality. A 2.2 µm oxide cladding

was deposited using a plasma-enhanced chemical vapour deposition (PECVD) process based on tetraethyl orthosilicate (TEOS) at 300°C. Reflectometry measurements were performed throughout the process to verify the device layer, buffer oxide and cladding thicknesses before delivery.

6. Experimental Data

To characterize the devices, a custom-built automated test setup [1, 3] with automated control software written in Python was used [4]. An Agilent 81600B tunable laser was used as the input source and Agilent 81635A optical power sensors as the output detectors. The wavelength was swept from 1500 to 1600 nm in 10 pm steps. A polarization maintaining (PM) fibre was used to maintain the polarization state of the light, to couple the TE polarization into the grating couplers [5]. A 90° rotation was used to inject light into the TM grating couplers [5]. A polarization maintaining fibre array was used to couple light in/out of the chip [6].

6.1. Baseline Correction

Raw measurement data includes the spectral response of the grating couplers and the propagation loss of the waveguides. To isolate the interference characteristics of the MZIs, the raw spectra were normalized using the transmission data from the reference straight waveguides.

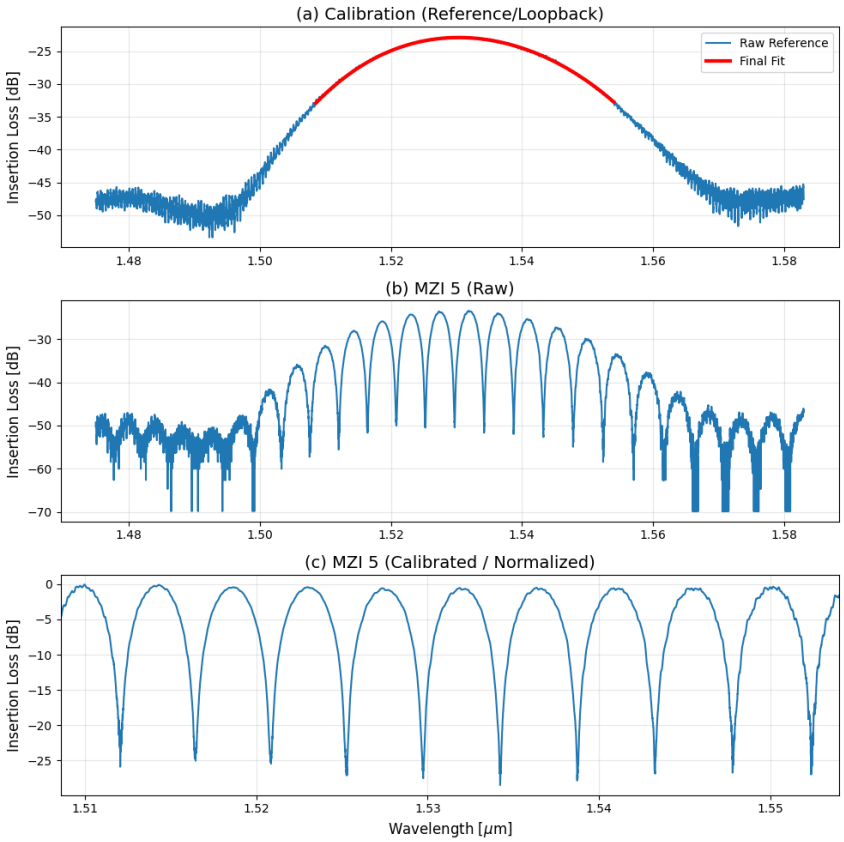

Fig. 10. Baseline correction process. The raw MZI spectrum (b) is normalized by the reference waveguide spectrum (a) to remove grating coupler envelope effects. (c) Shows the normalized MZI spectrum.

Fig. (10) (a) illustrates the raw spectral response of a reference waveguide compared to (b) the response of an MZI ($\Delta L = 100$ µm). A polynomial fit of the reference envelope was used to flatten the MZI response, resulting in the normalized transmission spectra used for analysis (c).

7. Measurement Data Analysis

7.1. Spectral Analysis

The normalized transmission spectra for the fabricated MZIs were analyzed to extract the Free Spectral Range (FSR) and the group index (n_g). Fig. (11) displays the measured transmission for the MZI with $\Delta L = 100$ µm, showing a clear interference pattern with high extinction ratios, indicating well-balanced power splitting in the Y-branches. Equation 12 shows the results of the fit for the compact model for the MZI with $\Delta L = 100$ µm.

$$n_{\text{eff}}(\lambda) = 2.4132 - 1.1556(\lambda - 1.55) - 0.042(\lambda - 1.55)^2 \tag{12}$$

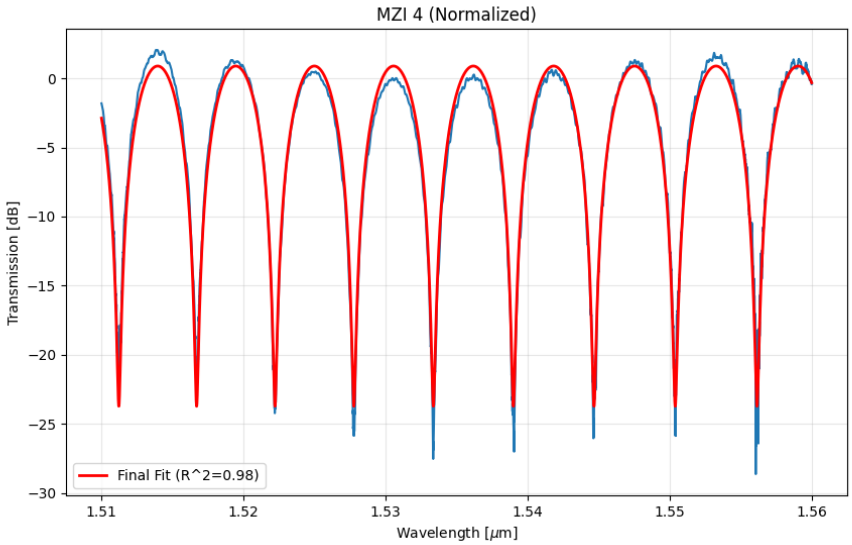

Fig. 11. Normalized transmission spectrum of the MZI with $\Delta L = 100$ µm. The FSR is indicated by the spacing between adjacent peaks.

7.2. Group Index Extraction

The group index was extracted from the experimental FSR using the relationship derived in Equation 10. Table 2 compares the theoretical FSR (simulated) with the experimentally measured FSR and the extracted group index at $\lambda = 1550$ nm.

7.3. Discussion

The experimental results show good agreement with the design simulations. The extracted group index oscillates around 4.186, which represents a deviation of approximately 0.26% from the simulated value of 4.197.

This discrepancy can be attributed to fabrication deviations, particularly in waveguide width. A variation in width changes the modal confinement and, consequently, the group index.

Table 2. Comparison of Simulated vs. Measured Results

Design #	**ΔL** (µm)	**Sim. FSR**	**Meas. FSR**	**Extracted n_g**	**Error** (%)
1	25	22.89	22.54	4.1996	1.53
2	50	11.45	11.19	4.1832	2.27
3	75	7.63	7.46	4.1817	2.23
4	100	5.72	5.59	4.1862	2.27
5	125	4.58	4.48	4.1802	2.18

8. Conclusion

We successfully designed, fabricated, and characterized a set of silicon photonic Mach-Zehnder Interferometers. The devices were modeled using Lumerical MODE and INTERCONNECT to determine the waveguide geometry and predict circuit behavior.

Experimental characterization confirmed the validity of the design. The measured Free Spectral Ranges followed the expected inverse relationship with path length difference (ΔL). The extracted group indices showed a variance of less than 2.3% compared to simulations, validating the fabrication quality and the accuracy of the compact models used. Deviations were analyzed and attributed to standard lithographic tolerances.

Future work could involve designing thermally tunable MZIs by integrating micro-heaters to actively control the phase shift, allowing for reconfigurable optical switching and modulation.

Disclosures. The authors declare no conflicts of interest.

References

1. L. Chrostowski and M. Hochberg, *Silicon Photonics Design: From Devices to Systems* (Cambridge University Press, 2015).
2. Ansys Lumerical, "Photonics simulation software," https://www.ansys.com/products/photonics (2024). Accessed: September 23, 2024.
3. "Maple Leaf Photonics," http://mapleleafphotonics.com. Seattle WA, USA.
4. "Automated probe station control software," http://siepic.ubc.ca/probestation. Python code developed by Michael Caverley.
5. Y. Wang, X. Wang, J. Flueckiger, *et al.*, "Focusing sub-wavelength grating couplers with low back reflections for rapid prototyping of silicon photonic circuits," Opt. Express **22**, 20652–20662 (2014).
6. "PLC Connections," www.plcconnections.com. Columbus OH, USA.